Available online at www.sciencedirect.com
SCIENCE DIRECT
Journal of Sound and Vibration 297 (2006) 106–122
JOURNAL OF SOUND AND VIBRATION
www.elsevier.com/locate/jsvi

Transient dynamic response of tubes to internal detonation loading

K. Mazaheri*, M. Mirzaei, H. Biglari

Department of Mechanical Engineering, Tarbiat Modares University, Tehran, Iran

Received 6 April 2005; received in revised form 13 March 2006; accepted 16 March 2006
Available online 5 June 2006

Abstract

This paper reports the analytical and numerical modeling of transient–dynamic response of tubes to internal detonation loading. Since gaseous detonation involves loads that propagate at high speeds, the excitations of flexural waves in the tube wall become significant. Flexural waves can result in high strains, which may exceed the equivalent static strains by up to a factor of 4. The presented analytical model, which considers the effects of transverse shear and rotary inertia, provides a very good simulation of the structural response of cylindrical tubes with finite length to internal detonation loading. It is shown that the predictions provided by this model are in better agreement with the experimental results, as compared to the existing analytical models. In the numerical part of this study, several finite element analyses are carried out to obtain the structural response of the tube to pressure loads moving at different speeds. The results of the analytical and numerical simulations are compared with experimental results reported in the literature.

1. Introduction

A detonation consists of a shock wave and a reaction zone that are tightly coupled. An ideal detonation travels at a nearly constant speed close to the Chapman–Jouguet velocity (V_{cj}), which is between 1500 and 3000 m/s in gases depending on the fuel–oxidizer combination. The pressure just behind the detonation can be as high as 20–30 times the ambient pressure. A typical experimental pressure–time trace and an ideal profile for a detonation are shown in Fig. 1 [1]. The almost instantaneous jump in pressure at time zero corresponds to the passage of the detonation wave past the measuring point. The more gradual decrease in pressure up to 0.25 ms and the plateau for longer times are associated with the gas dynamics of the flow behind the wave. The pressure history for this type of loading may be represented by an exponential approximation to the Taylor–Zeldovich model and can be characterized by the initial pressure p_1, the peak pressure p_2, the final pressure p_3, the exponential decay factor T, and the velocity V_{cj} [1] as follows:

$$p(t) = (p_1 - p_{atm}) + [(p_3 - p_1) + (p_2 - p_3)e^{-t/T}][1 - H(x - V_{cj}t)]. \quad (1)$$

*Corresponding author. Fax: +98 21 8800 5040.
E-mail address: kiumars@modares.ac.ir (K. Mazaheri).

0022-460X/$ - see front matter © 2006 Elsevier Ltd. All rights reserved.
doi:10.1016/j.jsv.2006.03.027

Nomenclature

$A0$	dispersion premultiplication factor, dimensionless
$A2$	dispersion premultiplication factor, dimensionless
$A4$	dispersion premultiplication factor, dimensionless
E	Young's modulus, N/m^2
F	dimensionless loading function, dimensionless
F_d	dimensionless dynamic loading function, dimensionless
F_s	dimensionless static loading function, dimensionless
G	shear modulus, N/m^2
h	shell thickness, m
L	length of shell, m
n	mode index, dimensionless
N	parameter defined in Eq. (29)
p_1	pre-detonation pressure, Pa
p_2	maximum-detonation pressure, Pa
p_3	post-shock pressure, Pa
p_{atm}	atmospheric pressure, Pa
p_{cj}	Chapman–Jouguet pressure, Pa
R	shell mean radius, m
R_{in}	inner radius of shell, m
R_{out}	outer radius of shell, m
t	time, s
T	exponential decay factor, s
T_n	Time-dependent part of the solution (s)
u	axial deflection, m
$\overline{u}$	dimensionless axial deflection, dimensionless
V	load speed, m/s
V_{c0}	critical velocity, m/s
V_{c1}	shear wave velocity, m/s
V_{c2}	dilatational wave velocity in a bar, m/s
V_{c3}	dilatational wave velocity, m/s
V_{cj}	Chapman–Jouguet velocity, m/s
V_d	dilatational wave speed, m/s
V_s	shear wave speed, m/s
w	radial deflection, m
$\overline{w}$	dimensionless radial deflection, dimensionless
$\overline{w}_b$	dimensionless radial deflection, bending, dimensionless
$\overline{w}_b^{\mathrm{I}}$	dimensionless radial deflection region I, dimensionless
$\overline{w}_b^{\mathrm{II}}$	dimensionless radial deflection region II, dimensionless
x	axial coordinate, m
X_n	eigenmodes, dimensionless
β	shell thickness parameter, dimensionless
$\overline{\eta}$	dimensionless (moving) axial coordinate, dimensionless
κ	shear correction factor, dimensionless
Λ_j	excitation parameter ($j = 1, 2, 3$), dimensionless
Λ_j^d	excitation parameter ($j = 1, 2, 3$), dimensionless
Λ_j^s	excitation parameter ($j = 1, 2, 3$), dimensionless
ν	Poisson's ratio, dimensionless
ρ	density, kg/m^3

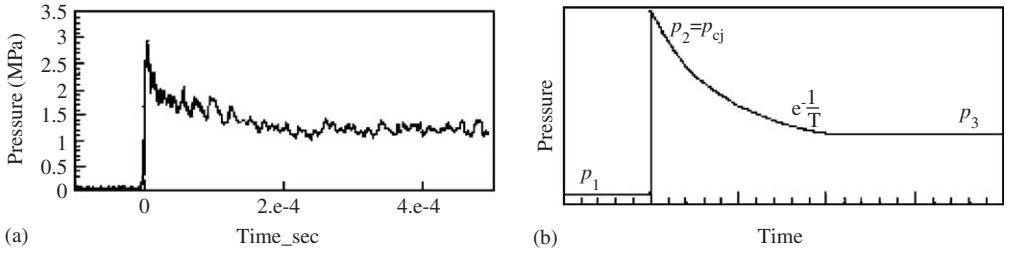

Fig. 1. Pressure versus time for detonation loading: (a) measured; (b) ideal model [1].

In the above equation, p_{atm} is the atmospheric pressure, x is the distance variable, t is the time variable and H is the step function.

Static pressure vessel design starts by considering the deflections that will be produced by a given internal pressure. Under dynamic loading conditions, the actual deflections will be further amplified by response of the

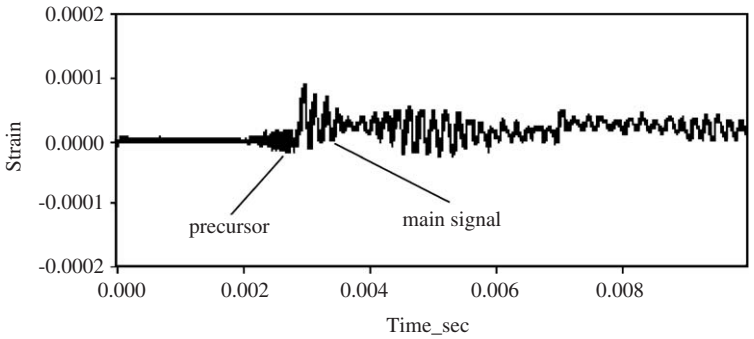

Fig. 2. Example of circumferential strain versus time for detonation loading. The interference patterns are due to the reflected waves associated with the clamp at nearby end of the tube segment [1].

structure to a time-dependent load. Therefore, an important factor in design for dynamic loading is the amplification factor, which is defined as the ratio of the maximum strain to the static strain for the same nominal loading pressure (Chapman–Jouguet pressure). The amplification factor, also referred to as the dynamic load factor, may be defined as

$$\text{Amp.Fac.} = \frac{w_{\text{dyn,max}}}{w_{\text{st}}}. \tag{2}$$

For simple structures that can be described with a single degree of vibrational freedom, the highest value that the amplification factor can assume is 2. However, for a continuous structure with a traveling load, no such simple estimate appears to be possible and more detailed considerations are needed.

From the structural point of view, the tube in which the detonation occurs experiences a traveling internal load that produces transient deformations. Fig. 2 shows the measured circumferential strain as a function of time for a tube with internal detonation loading [1]. The strain history shows a sharp peak when the detonation passes the measurement point (at $t = 2.9$ ms). For detonation loading, the circumferential strain can exceed the equivalent static strain (obtained for the tube under the static pressure P_{cj}) by up to a factor of 3–4. Such experimental results indicate that a simple static model of the tube cross-section is not sufficient for describing the dynamic nature of the strain distribution in the tube.

There have been several investigations dealing with the structural response of shells to internal shock or detonation loading [2–10], a brief review of those can be found in Ref. [1]. The first comprehensive theories for predicting the elastic response of a tube to a moving load were developed by Tang [11] and Reismann [12]. Tang [11] presented a model to predict the response of a thin shell to internal shock loading. By assuming a tube of infinite length, the problem was reduced to a "steady state" problem and an analytical solution for the shell motion was obtained. This model predicts the existence of a so-called critical velocity. When the pressure load travels at this critical speed, the solution for the radial tube motion becomes unbounded. Reismann [12] developed a model that includes the effect of prestress on the structural response and gave an elegant explanation of how the resonant coupling between a moving load and the flexural waves comes about [1].

2. Analytical models

We start this section with a brief review of some of the available analytical models including the *thin infinite shell with rotary inertia and shear deformation* (Tang model), and the *transient model without rotary inertia and shear deformation* [13]. In sequel, the validity of a new transient model for *a finite tube*, *which includes the effects of rotary inertia and shear deformation* [14], will be investigated through comparisons with experimental results reported in the literature and finite element simulations.

2.1. Thin infinite shell including rotary inertia and shear deformation (Tang model)

Tang's model [11] is based on a thin-shell *approximation,* but includes the effects of rotary inertia and transverse shear deformation. In this model, the detonation loading with a definite pressure profile moves with constant speed (V_{cj}) along the tube. The model is steady state in the sense that the transient development of the tube deformation is ignored and the response is assumed to be time-independent in the frame of reference of the detonation front. The model provides an analytical solution for the deformation, which exhibits the excitation of flexural waves and the existence of a critical speed. However, the response is obviously unrealistic (unbounded) at the critical speed and such features of real tubes as finite length and supports or flanges cannot be handled.

We start with the definition of the following dimensionless quantities which will facilitate the derivation of the equations:

$$\overline{u} = \frac{u}{h}, \quad \overline{w} = \frac{w}{h}, \quad \overline{\eta} = \frac{\sqrt{12}}{h}(x - Vt) \tag{3}$$

in which u and w are the longitudinal and radial displacements respectively, and h is the shell thickness.

In fact, by introducing $\overline{\eta}$, the two variables x and t are combined into one variable. As shown in the Fig. 3, two regions can be distinguished in the tube. In region I, $\overline{\eta}<0$ and the detonation front has passed the points in this region. In region II, $\overline{\eta}>0$ and the detonation front has not yet arrived.

The following parameters are used in the analysis:

$$\Lambda_i = \frac{p_i R^2}{Eh^2} \quad \text{excitation parameters } (j = 1, 2 \text{ or } 3),$$

$$V_d = \sqrt{\frac{E}{\rho(1-\nu^2)}} \quad \text{dilatational wave velocity},$$

$$V_s = \sqrt{\frac{\kappa G}{\rho}} \quad \text{shear wave velocity},$$

$$\beta = \frac{h}{\sqrt{12}R} \quad \text{shell thickness parameter}.$$

Using the above variables and parameters, the following differential equation can be considered to govern the structural response of the tube in the Tang model [13]

$$A_4 \frac{\partial^4 \overline{w}}{\partial \overline{\eta}^4} + A_2 \frac{\partial^2 \overline{w}}{\partial \overline{\eta}^2} + A_0 \overline{w} = F(\overline{\eta}), \tag{4}$$

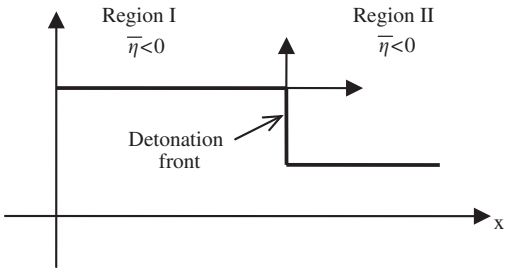

Fig. 3. Dimensionless variable $\overline{\eta}$.

where the coefficients are given by

$$A_4 = \left[\left(V/V_d\right)^2 - 1\right]\left[\left(V/V_s\right)^2 - 1\right],$$
$$A_2 = \left(V/V_d\right)^2\left[1 + \beta^2\left(V_d/V_s\right)^2\right] - \beta^2\left(1 - v^2\right)\left(V_d/V_s\right)^2,$$
$$A_0 = \beta^2 + \frac{\beta^2 v^2}{\left[\left(V/V_d\right)^2 - 1\right]},$$
$$F(\overline{\eta}) = \left(1 - v^2\right)\beta^2\left[\Lambda_1 + (\Lambda_3 - \Lambda_1)(1 - H(\overline{\eta})) + (\Lambda_2 - \Lambda_3)\mathrm{e}^{\overline{\eta}/\eta_0}(1 - H(\overline{\eta}))\right]. \tag{5}$$

In these expressions, $H(\overline{\eta})$ is the step function and $\overline{\eta}_0 = \sqrt{12}VT/h$.

By solving the dispersion equation, four critical velocities are obtained:

- V_{C0}: the value of the critical velocity V_{C0} can be calculated from the vanishing of the discriminant $A_2^2 - 4A_0A_4 = 0$.
- V_{C1}: the shear wave speed V_s.
- V_{C2}: the dilatational wave speed in a bar $V_d\sqrt{1 - v^2}$.
- V_{C3}: the dilatational wave speed V_d.

Based on the values of the speed V, five different cases can be distinguished. In the present investigation, only the first two are relevant. In the first case, $0 < V < V_{C0}$; the values of α (roots of characteristic equation) are complex: $\alpha = \pm n \pm im$. In the second case, $V_{C0} < V < V_{C1}$, the values of α are purely imaginary: $\alpha = \pm im_1$ and $\alpha = \pm im_2$.

2.1.1. Case 1: $0 < V < V_{C0}$

In this case, flexural displacements of the tube in the regions I and II are

$$\begin{aligned}
\overline{w}_b^{\mathrm{I}} = {} & \frac{n^2 - m^2}{4nm}\left[\left(\Lambda_3^s - \Lambda_1^s\right) + \left(\Lambda_2^d - \Lambda_3^d\right)\right]\mathrm{e}^{n\overline{\eta}}\sin m\overline{\eta} \\
& + \left[\frac{-1}{2}\left(\Lambda_3^s - \Lambda_1^s\right) + \frac{-1}{2}\left(\Lambda_2^d - \Lambda_3^d\right)\right]\mathrm{e}^{n\overline{\eta}}\cos m\overline{\eta} \\
& + \left(\Lambda_2^d - \Lambda_3^d\right)\left(\frac{-1}{4m(n^2 + m^2)}\frac{1}{\overline{\eta}_0^3} - \frac{1}{4nm}\frac{1}{\overline{\eta}_0^2} + \frac{n^2 - 3m^2}{4m(n^2 + m^2)}\frac{1}{\overline{\eta}_0}\right)\mathrm{e}^{n\overline{\eta}}\sin m\overline{\eta} \\
& + \frac{\left(\Lambda_2^d - \Lambda_3^d\right)}{4n(n^2 + m^2)}\left(\frac{1}{\overline{\eta}_0^3} + \frac{m^2 - 3n^2}{\overline{\eta}_0}\right)\mathrm{e}^{n\overline{\eta}}\cos m\overline{\eta} + \Lambda_3^s + \left(\Lambda_2^d - \Lambda_3^d\right)\mathrm{e}^{\overline{\eta}/\overline{\eta}_0}, \\
\overline{w}_b^{\mathrm{II}} = {} & \frac{n^2 - m^2}{4nm}\left[\left(\Lambda_3^s - \Lambda_1^s\right) + \left(\Lambda_2^d - \Lambda_3^d\right)\right]\mathrm{e}^{-n\overline{\eta}}\sin m\overline{\eta} \\
& + \left[\frac{1}{2}\left(\Lambda_3^s - \Lambda_1^s\right) + \frac{1}{2}\left(\Lambda_2^d - \Lambda_3^d\right)\right]\mathrm{e}^{-n\overline{\eta}}\cos m\overline{\eta} \\
& + \left(\Lambda_2^d - \Lambda_3^d\right)\left(\frac{1}{4m(n^2 + m^2)}\frac{1}{\overline{\eta}_0^3} - \frac{1}{4nm}\frac{1}{\overline{\eta}_0^2} - \frac{n^2 - 3m^2}{4m(n^2 + m^2)}\frac{1}{\overline{\eta}_0}\right)\mathrm{e}^{-n\overline{\eta}}\sin m\overline{\eta} \\
& + \frac{\left(\Lambda_2^d - \Lambda_3^d\right)}{4n(n^2 + m^2)}\left(\frac{1}{\overline{\eta}_0^3} + \frac{m^2 - 3n^2}{\overline{\eta}_0}\right)\mathrm{e}^{-n\overline{\eta}}\cos m\overline{\eta} + \Lambda_1^s.
\end{aligned} \tag{6}$$

2.1.2. Case 2: $V_{C0} < V < V_{C1}$

Here, the flexural displacements of the tube in the regions I and II are

$$\begin{aligned}
\overline{w}_b^{\mathrm{I}} = {} & \frac{1}{m_1\left(m_1^2 - m_2^2\right)}\left(m_2^2 + \frac{1}{\overline{\eta}_0^2}\right)\frac{1}{\overline{\eta}_0}\left(\Lambda_2^d - \Lambda_3^d\right)\sin m_1\overline{\eta} + \Lambda_3^s + \left(\Lambda_2^d - \Lambda_3^d\right)\mathrm{e}^{\overline{\eta}/\overline{\eta}_0} \\
& + \left(\frac{m_2^2}{m_1^2 - m_2^2}\left(\Lambda_3^s - \Lambda_1^s\right) + \frac{m_2^2}{m_1^2 - m_2^2}\left(\Lambda_2^d - \Lambda_3^d\right) + \frac{1}{m_1^2 - m_2^2}\frac{1}{\overline{\eta}_0^2}\left(\Lambda_2^d - \Lambda_3^d\right)\right)\cos m_1\overline{\eta},
\end{aligned}$$

$$\overline{w}_b^{\mathrm{II}} = \frac{1}{m_2(m_1^2 - m_2^2)}\left(m_1^2 + \frac{1}{\overline{\eta}_0^2}\right)\frac{1}{\overline{\eta}_0}\left(\Lambda_2^d - \Lambda_3^d\right)\sin m_2\overline{\eta} + \Lambda_1^s + \left(\frac{m_1^2}{m_1^2 - m_2^2}\left(\Lambda_3^s - \Lambda_1^s\right) + \frac{m_1^2}{m_1^2 - m_2^2}\left(\Lambda_2^d - \Lambda_3^d\right) + \frac{1}{m_1^2 - m_2^2}\frac{1}{\overline{\eta}_0^2}\left(\Lambda_2^d - \Lambda_3^d\right)\right)\cos m_2\overline{\eta}. \tag{7}$$

In Eqs. (6) and (7) the parameters Λ_i^s and Λ_i^d are

$$\Lambda_i^s = \frac{\beta^2(1-\nu^2)(\Lambda_i - \Lambda_{\mathrm{atm}})}{A_0}, \quad \Lambda_i^d = \frac{\beta^2(1-\nu^2)(\Lambda_i - \Lambda_{\mathrm{atm}})}{\left(A_4/\overline{\eta}_0^4 + A_2/\overline{\eta}_0^2 + A_0\right)}. \tag{8}$$

2.2. Transient model I [1]

The "steady state" model has severe limitations for making realistic predictions, particularly near the critical velocity, where the response is predicted to be infinite. The most accurate quantitative method to solve this problem is to use the finite element method (FEM). A less accurate but somewhat simpler method is to consider additional simplifications to the model and simplify the governing equation so that the classical methods of analysis can be used to construct a time-dependent solution. The simplifications for Model I were to *neglect the effects of transverse shear and rotary inertia* which is equivalent to taking $V_s \to \infty$ and $V/V_d \ll 1$ [1]. Accordingly, the solution was obtained as an infinite series of normal modes with time-dependent coefficients computed from the prescribed loading function. The complete solution for the specific cases of a finite length thin shell with either simply supported or clamped end conditions can be found in Ref. [1]. As a starting point for the analytical transient model, the following equation was used [13]:

$$\frac{\partial^4 w}{\partial x^4} + \frac{12}{h^2 V_d^2}\frac{\partial^2 w}{\partial t^2} + \frac{12^2\beta^2(1-\nu^2)}{h^4}w = \frac{12^2}{h^3}F(x,t). \tag{9}$$

Here $F(x, t)$ is the transient loading function. For detonation loading, $F(x, t)$ is

$$F(x,t) = \beta^2(1-\nu^2)\Lambda_1 + \beta^2(1-\nu^2)[(\Lambda_3 - \Lambda_1) + (\Lambda_2 - \Lambda_3)\mathrm{e}^{(x-Vt)/VT}](1 - H(x - Vt)). \tag{10}$$

The complete solution of the above equation can be found in Ref. [1].

2.3. Transient model II

In this section, the solution for the general problem is considered and applied to the specific case of a finite-length thin tube with simply supported condition.

Using Eqs. (4) and (5), the following governing equation can be developed for modeling the analytical transient behavior of the tube [14].

$$\frac{\partial^4 w}{\partial x^4} + \frac{1}{V_d^2 V_s^2}\frac{\partial^4 w}{\partial t^4} - \left(\frac{1}{V_d^2} + \frac{1}{V_s^2}\right)\frac{\partial^4 w}{\partial x^2 \partial t^2} + \frac{12}{h^2 V_d^2}\left(1 + \beta^2\frac{V_d^2}{V_s^2}\right)\frac{\partial^2 w}{\partial t^2}, - \frac{12\beta^2(1-\nu^2)}{h^2}\frac{V_d^2}{V_s^2}\frac{\partial^2 w}{\partial x^2} + \frac{12^2\beta^2}{h^4}\left(1 - \frac{\nu^2}{1-(V/V_d)^2}\right)w = \frac{12^2}{h^3}F(x,t).$$

$$\begin{cases} w(0,t) = w(L,t) = 0, \\ \left.\dfrac{\partial^2 w}{\partial x^2}\right|_{x=0} = \left.\dfrac{\partial^2 w}{\partial x^2}\right|_{x=L} = 0, \end{cases} \quad \begin{cases} w(x,0) = w_s, \\ \left.\dfrac{\partial w}{\partial t}\right|_{t=0} = 0, \end{cases} \tag{11}$$

where $w = \overline{w}h$, $F(x, t)$ is the transient loading function, and w_s is the initial deflection due to static loading. Now we will examine the coefficient of the second term of the above equation in more detail

$$\frac{1}{V_d^2 V_s^2} = \frac{\rho^2}{E^2}\frac{2(1+\nu)^2(1-\nu)}{\kappa}. \tag{12}$$

It turns out that the value of this coefficient is on order of 1×10^{-13} and we may ignore it without any loss of generality. In order to simplify the solution procedure we may define the following parameters:

$$a^2 = \frac{1}{V_d^2} + \frac{1}{V_s^2}, \quad b^2 = \frac{12}{h^2 V_d^2}\left(1 + \beta^2 \frac{V_d^2}{V_s^2}\right), \quad c^2 = \frac{12\beta^2(1-\nu^2)}{h^2}\frac{V_d^2}{V_s^2},$$
$$e^2 = \frac{12^2\beta^2}{h^4}\left(1 - \frac{\nu^2}{1-(V/V_d)^2}\right), \quad q(x,t) = \frac{12^2}{h^3}F(x,t). \tag{13}$$

Accordingly, Eq. (11) can be written as

$$\frac{\partial^4 w}{\partial x^4} - a^2\frac{\partial^4 w}{\partial x^2 \partial t^2} + b^2\frac{\partial^2 w}{\partial t^2} - c^2\frac{\partial^2 w}{\partial x^2} + e^2 w = q(x,t). \tag{14}$$

For detonation loading Eq. (10) is used. Eq. (14) may be solved using the technique of separation of variables by writing the general form of the solution as an expansion of eigenmodes:

$$w(x,t) = \sum_{n=1}^{\infty} T_n(t) X_n(x). \tag{15}$$

In which $X_n(x)$ are the eigenmodes and $T_n(t)$ is the time-dependent part of the solution.
The eigenmodes can be obtained by solving the following differential equation:

$$\frac{\mathrm{d}^4 X_n}{\mathrm{d}x^4} + \lambda_{1n}\frac{\mathrm{d}^2 X_n}{\mathrm{d}x^2} + \lambda_{2n} X_n = 0. \tag{16}$$

The solution can be shown to be

$$X_n = C_1 \mathrm{e}^{Ax} + C_2 \mathrm{e}^{-Ax} + C_3 \mathrm{e}^{Bx} + C_4 \mathrm{e}^{-Bx}. \tag{17}$$

The coefficients C_i in Eq. (17) can be obtained based on the boundary conditions of the problem (Eq. (11)) and the orthonormality property of eigenmodes. The result gives

$$X_n = \sqrt{\frac{2}{L}}\sin\left(\frac{n\pi}{L}x\right), \quad n = 1, 2, \ldots \tag{18}$$

Having obtained the eigenmodes, we proceed towards finding the solution of the non-homogenous form of Eq. (14). We may expand $q(x,t)$ in terms of the eigenmodes as

$$q(x,t) = \sum_{n=1}^{\infty} Q_n(t) X_n(x). \tag{19}$$

Due to the orthonormality of eigenmodes the coefficients can be found from

$$Q_n(t) = \int_0^L q(x,t) X_n(x)\,\mathrm{d}x. \tag{20}$$

Substituting for $q(x,t)$ into (14) we may write

$$\left(-a^2\frac{\mathrm{d}^2 X_n}{\mathrm{d}x^2} + b^2 X_n\right)\frac{\mathrm{d}^2 T_n(t)}{\mathrm{d}t^2} + \left(-\lambda_n\frac{\mathrm{d}^2 X_n}{\mathrm{d}x^2} - c^2\frac{\mathrm{d}^2 X_n}{\mathrm{d}x^2} + e^2 X_n\right) T_n(t) = Q_n X_n. \tag{21}$$

From Eq. (18) we may conclude that

$$\frac{\mathrm{d}^2 X_n}{\mathrm{d}x^2} = -\lambda_n X_n. \tag{22}$$

Substituting the above equation into Eq. (21) results in

$$(a^2\lambda_n + b^2)\frac{\mathrm{d}^2 T_n(t)}{\mathrm{d}t^2} + (\lambda_n^2 + c^2\lambda_n + e^2) T_n(t) = Q_n \tag{23}$$

which in combination with Eq. (20) will give the following differential equation for the time-dependent part of the general solution

$$\frac{\mathrm{d}^2 T_n(t)}{\mathrm{d}t^2} + \omega_n^2 T_n(t) = \frac{\int_0^L q(x,t) X_n(x)\,\mathrm{d}x}{a^2\lambda_n + b^2}. \tag{24}$$

In the above we have

$$\omega_n = \sqrt{\frac{\lambda_n^2 + c^2\lambda_n + e^2}{a^2\lambda_n + b^2}}. \tag{25}$$

The solution of the above equation comprises of the homogenous and the non-homogenous parts. The homogenous solution is

$$T_n(t) = A_n \sin(\omega_n t) + B_n \cos(\omega_n t). \tag{26}$$

In order to find the non-homogenous solution, we divide the load function into the static and dynamic parts. The static part of the detonation loading obtained from Eq. (10) is

$$q_{\mathrm{ns}} = \frac{12^2}{h^3}\beta^2(1-v^2)\Lambda_1. \tag{27}$$

Hence the static part of the non-homogenous solution would be

$$T_{\mathrm{ns}} = \left(\frac{N}{\omega_n^2}\right)\Lambda_1(1-\cos(n\pi)) \tag{28}$$

in which N is

$$N = \sqrt{\frac{2}{L}}\frac{12^2\beta^2(1-v^2)}{h^3(a^2\lambda_n + b^2)}\frac{L}{n\pi}. \tag{29}$$

The dynamic part of the detonation loading would be

$$q_d(t) = \frac{12^2}{h^3}\beta^2(1-v^2)\left[(\Lambda_3-\Lambda_1) + (\Lambda_2-\Lambda_3)\mathrm{e}^{(x-Vt)/VT}\right]. \tag{30}$$

Accordingly, the dynamic part of the non-homogenous solution is

$$\begin{aligned} T_{\mathrm{nd}}(t) = {} & \frac{-N}{\left(\omega_n^2 - \left(\frac{n\pi V}{L}\right)^2\right)}\left[(\Lambda_3-\Lambda_1) + \frac{1}{1+\left(\frac{L}{n\pi VT}\right)^2}(\Lambda_2-\Lambda_3)\right]\cos\left(\frac{n\pi Vt}{L}\right) \\ & + \frac{N}{\left(\omega_n^2 - \left(\frac{n\pi V}{L}\right)^2\right)}\left[\frac{L}{n\pi VT}\frac{1}{1+\left(\frac{L}{n\pi VT}\right)^2}(\Lambda_2-\Lambda_3)\right]\sin\left(\frac{n\pi Vt}{L}\right) \\ & + \left[\frac{N}{\left(\omega_n^2 + \left(\frac{1}{T}\right)^2\right)}\frac{1}{1+\left(\frac{L}{n\pi VT}\right)^2}(\Lambda_2-\Lambda_3)\mathrm{e}^{-t/T} + \frac{N}{\omega_n^2}(\Lambda_3-\Lambda_1)\right]. \end{aligned} \tag{31}$$

The complete form of the time-dependent part of the general solution would be

$$T_n(t) = T_{\mathrm{ns}} + T_{\mathrm{nd}}(t) + A_n \sin(\omega_n t) + B_n \cos(\omega_n t). \tag{32}$$

The coefficients A_n and B_n can be obtained from the initial conditions and can be shown to be

$$A_n = \frac{NT}{\omega_n} \frac{\left(\frac{n\pi V}{L}\right)^2}{\left(\frac{n\pi V}{L}\right)^2 + \left(\frac{n\pi V}{L}\right)^2 \omega_n^2 T^2 - \omega_n^4 T^2 - \omega_n^2} ((\Lambda_2 - \Lambda_1) - (\Lambda_3 - \Lambda_1)),$$

$$B_n = -\frac{N}{\omega_n^2} \frac{\left(\frac{n\pi V}{L}\right)^2}{\left(\frac{n\pi V}{L}\right)^2 + \left(\frac{n\pi V}{L}\right)^2 \omega_n^2 T^2 - \omega_n^4 T^2 - \omega_n^2} ((\Lambda_3 - \Lambda_1) + \omega_n^2 T^2 (\Lambda_2 - \Lambda_1)). \tag{33}$$

Having found all the required terms, the general solution can be obtained from the following equation, along with Eqs. (28), (31) and (33).

$$w(x,t) = \sum_{n=1}^{\infty} \left[[T_{\text{ns}} + T_{\text{nd}}(t) + A_n \sin(\omega_n t) + B_n \cos(\omega_n t)] \sqrt{\frac{2}{L}} \sin\left(\frac{n\pi}{L} x\right) \right]. \tag{34}$$

3. Finite element simulations

In previous sections, analytical models were presented for the transient behavior of finite length tubes. An alternative approach is to use the FEM, which enables a more realistic modeling of geometries and boundary conditions. The finite element simulations were carried out using the LS-DYNA V960 package, which has wide abilities in solving dynamic problems. Several transient linear elastic analyses was carried out to calculate the structural response of the tube to a moving pressure load, using 500 rotary symmetric solid elements in the axial direction and five solid elements in the radial direction (Fig. 4).

The transient loading was represented by prescribing force as a function of time at each element (Fig. 5). The force history for each node was a discrete version of the exponential approximation to the Taylor–Zeldovich model. The moving load was simulated by considering the difference in detonation arrival time at each element. Calculations were carried out for a clamped tube and a simply supported tube (Fig. 4), where R_{in} is the internal radius of the tube. In these simulations the effects of reflection of structural waves were not considered. The results of the analyses are presented in subsequent sections.

4. Results and discussion

In this section the results obtained from Model II are compared with other analytical models, finite element results, and the experimental results reported in literature [1,13]. In these experiments a stoichiometric hydrogen–oxygen mixture with a variable amount of argon, as diluents, was used [1]. The amount of argon N_{Ar} was used to control the velocity of the detonation over a range of 1300–2800 m/s, bracketing the critical velocity. The material and geometrical properties of the tube are shown in Table 1, and the positions of strain gauges are depicted in Fig. 6 and listed in Table 2.

4.1. Representative strain histories

Experimental strain histories for gauges 5 and 10 are given in Fig. 7 [1]. Gauge 5 is mounted in the first half of the second tube section, 0.79 m from the entrance to that section, and gauge 10 is mounted near the end of the second tube section, 2.195 m from the entrance to that section. In Fig. 7, the top plot is the strain history for a subcritical velocity (1400.1 m/s), the middle plot is the strain history for a velocity around the critical velocity (1478.8 m/s), and the bottom plot is the supercritical strain history (1699.7 m/s). For detonation speeds of 1400.1, 1478.8, and 1699.7 m/s, it takes 5.10, 4.83, and 4.20 ms, respectively, to cover the length of the tube. The maximum pressures p_2, for the above speeds, are 1.2, 1.35 and 1.7 MPa respectively. For all

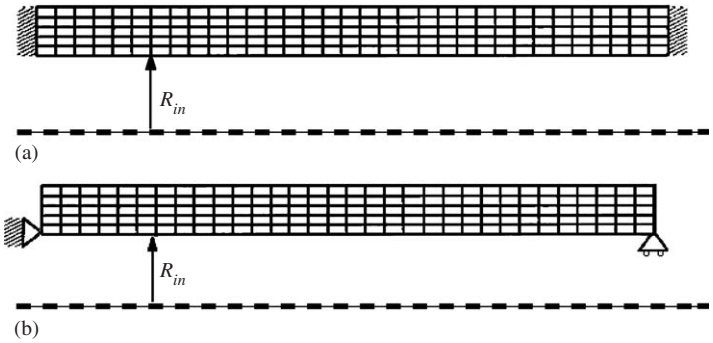

Fig. 4. Geometry and boundary conditions of the model: (a) clamped support and (b) simple support.

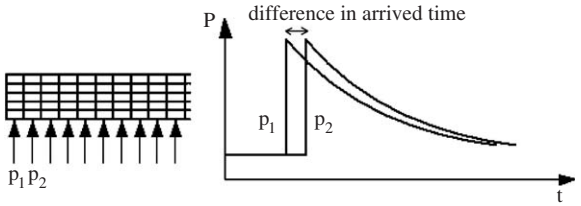

Fig. 5. Schematic of moving load.

cases, the initial pressure p_1 and final pressure p_3 are zero and $T = 4.34 \times 10^{-4}$. The spike or glitch at about 100 ms is actually due to the electric discharge used to start the detonation [1].

4.2. Verification of the models

Fig. 8 shows the circumferential strain versus time computed using the Tang model. Since the steady-state model gives results that are independent of gauge position, only one trace is shown for each velocity case. For this model the corresponding critical velocity is 1455 m/s. The critical velocity obtained from experimental results is 1450 m/s [1]. The difference between subcritical and supercritical cases is striking with the very high decay rates for all oscillations in the subcritical case. The precursor extends far ahead of the main signal in the supercritical case. The peak amplitudes of the strains are in reasonable agreement with observation [1].

Computations using the transient analytical models for gauges 5 and 10 are shown in Figs. 9 and 10, respectively. Note that the arrival times on the experimental plots are adjusted to be directly comparable with analytical results.

It is evident that the results obtained from transient models are much more realistic than the steady-state model and clearly show that the development of many features in the strain signals is a consequence of unsteady behavior. Both the development of the precursors in gauge 10 and the modulation of the oscillations of the main signal are predicted by the transient analytical models. As shown subsequently, the predicted amplitudes of the transient models are also in reasonable agreement with the experimental results.

Also note that, due to inclusion of the effects of transverse shear and rotary inertia, the predictions of Model II are in better agreement with the experimental results. For instance, it is seen from Fig. 10(b) that for the gauge 10 the vibrational spectrum of the main signal predicted by Model I resides above the line STRAIN = 0. Whereas the behavior predicted by Model II shows a very good agreement with the pattern of the experimental results.

Nevertheless there are some discrepancies between the experimental results and those predicted by Model II. These can be attributed to: (a) the effect of reflected flexural wave is not considered in the model and (b) the detonation tube is in fact a thick shell while this is a thin shell model.

Table 1
Material and geometrical properties of the tube [1]

ρ (kg/m^3)	E (N/m^2)	v	R_{out} (m)	R_{in} (M)	$3L$ (m)
8×10^3	193×10^9	0.23	0.1651	0.1397	7.14

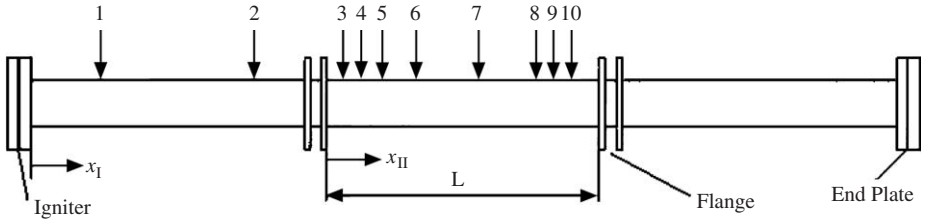

Fig. 6. Detonation tube and positions of strain gauges [1].

Table 2
Positions of strain gauges [1]

gauge	1	2						
x_I(m)	1.181	1.951						
gauge	3	4	5	6	7	8	9	10
x_{II}(m)	0.248	0.433	0.79	1.181	1.567	1.951	2.085	2.195

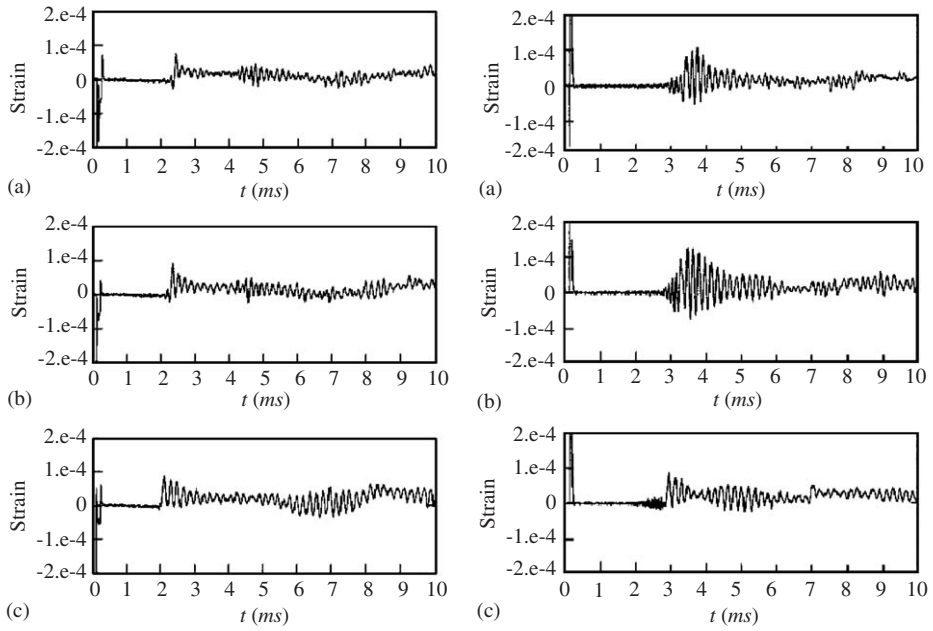

Fig. 7. Measured strain signals. Left gauge 5, and right gauge 10: (a) detonation velocity of 1400.1 m/s; (b) detonation velocity of 1478.8 m/s and (c) detonation velocity of 1699.7 m/s [1].

4.2.1. Comparison with FEM

The obtained results from FEM simulations, along with the results of transient analytical model II and the experimental results [1,13], are shown in Figs. 11 and 12 for gauges 5 and 10, respectively. Note that the arrival

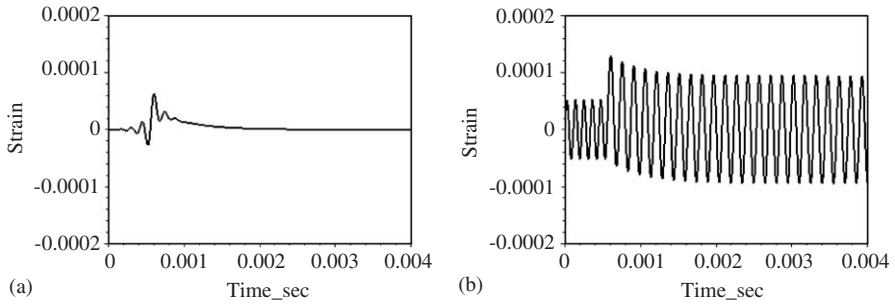

Fig. 8. Tang model strain predictions: (a) detonation velocity of 1400.1 m/s and (b) detonation velocity of 1478.8 m/s.

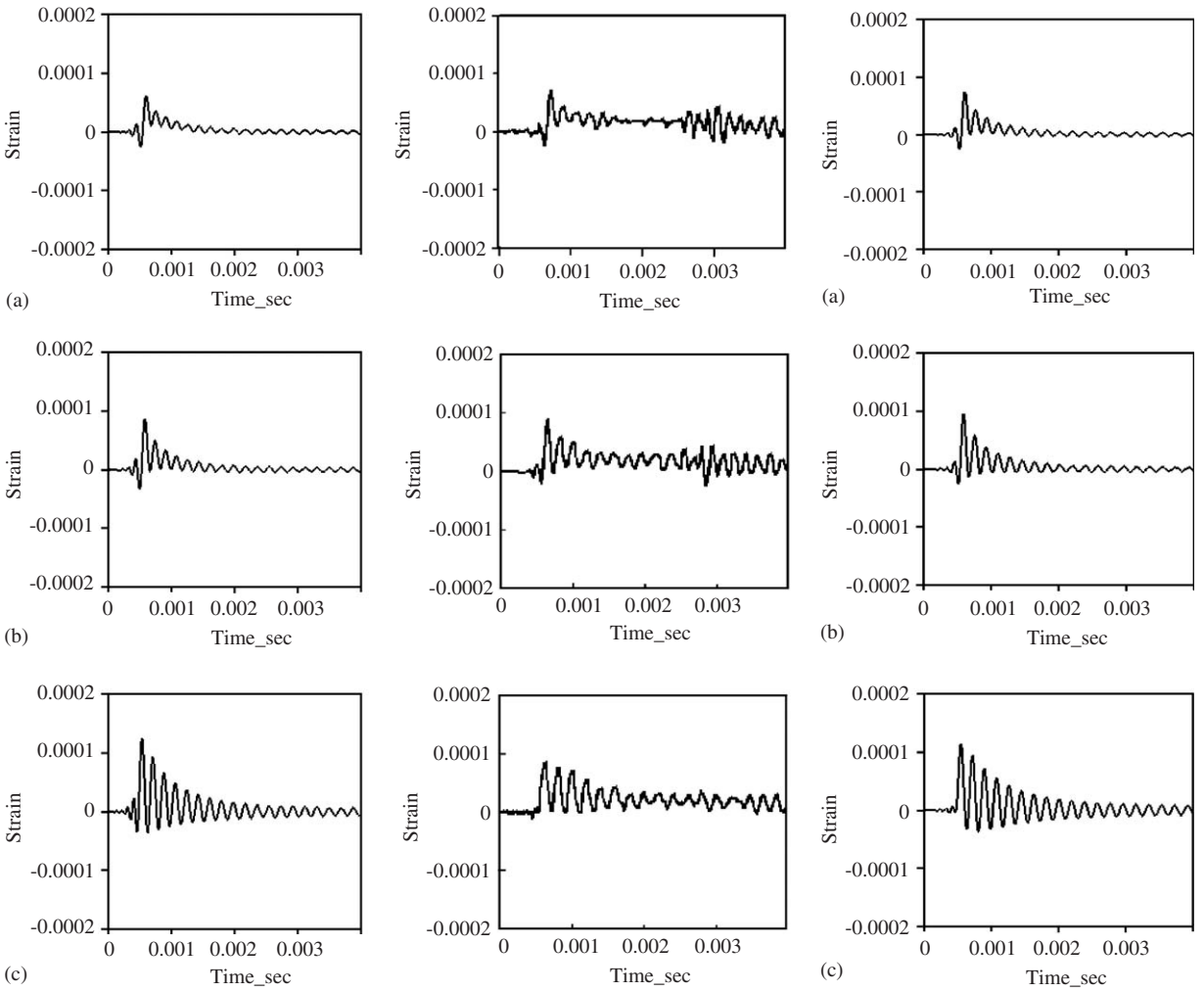

Fig. 9. Left column shows transient model I, right column shows transient model II, and middle column shows experimental strain predictions [1], for gauge 5: (a) detonation velocity of 1400.1 m/s; (b) detonation velocity of 1478.8 m/s; (c) detonation velocity of 1699.7 m/s.

times on the experimental plots are reduced to be comparable with the FEM and analytical results. Moreover, as it was observed that the FEM results obtained for the two different support conditions were the same, only the results for the simply supported case are reported. From the above figures it is clear that there is excellent

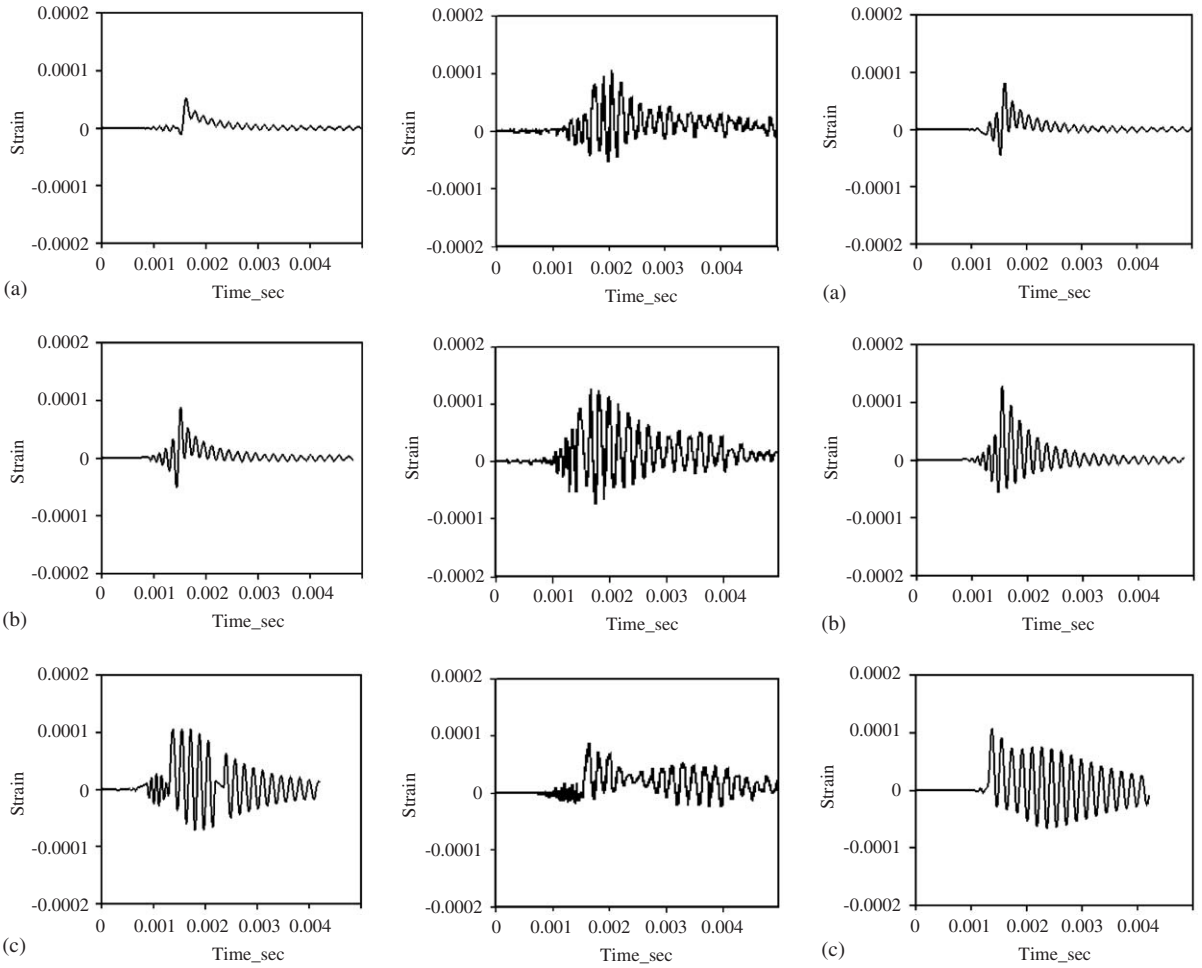

Fig. 10. Left column shows transient model I, right column shows transient model II, and middle column shows experimental strain predictions [1] for gauge 10: (a) detonation velocity of 1400.1 m/s; (b) detonation velocity of 1478.8 m/s and (c) detonation velocity of 1699.7 m/s.

agreement between the FEM results and the results of Model II. In general, the maximum strain amplitude obtained from FEM is in better agreement with the experiment. The discrepancies between the analytic (Model II) and FEM results with the experimental results may be attributed to the effects of reflected waves which were not considered in the former methods.

4.3. Amplifiicatiion factors

One of the main objectives of this investigation has been the determination of amplification factors. The amplification factor is a convenient way to represent the peak loads that can be expected and can be used by designers to incorporate the appropriate safety factors into the specification of piping systems that will be subjected to detonations.

The most important parameter in determining the amplification factor is the detonation wave speed. Amplification factors computed for four positions corresponding to gauges 3, 5, 7 and 10 (see Fig. 6) and wave speeds between 1300 and 2800 m/s, are shown in Fig. 13.

The results in Fig. 13 clearly demonstrate the transient nature of the process, the amplification factor develops as a function of distance. For strain gauge 3, flexural waves do not develop and critical velocity

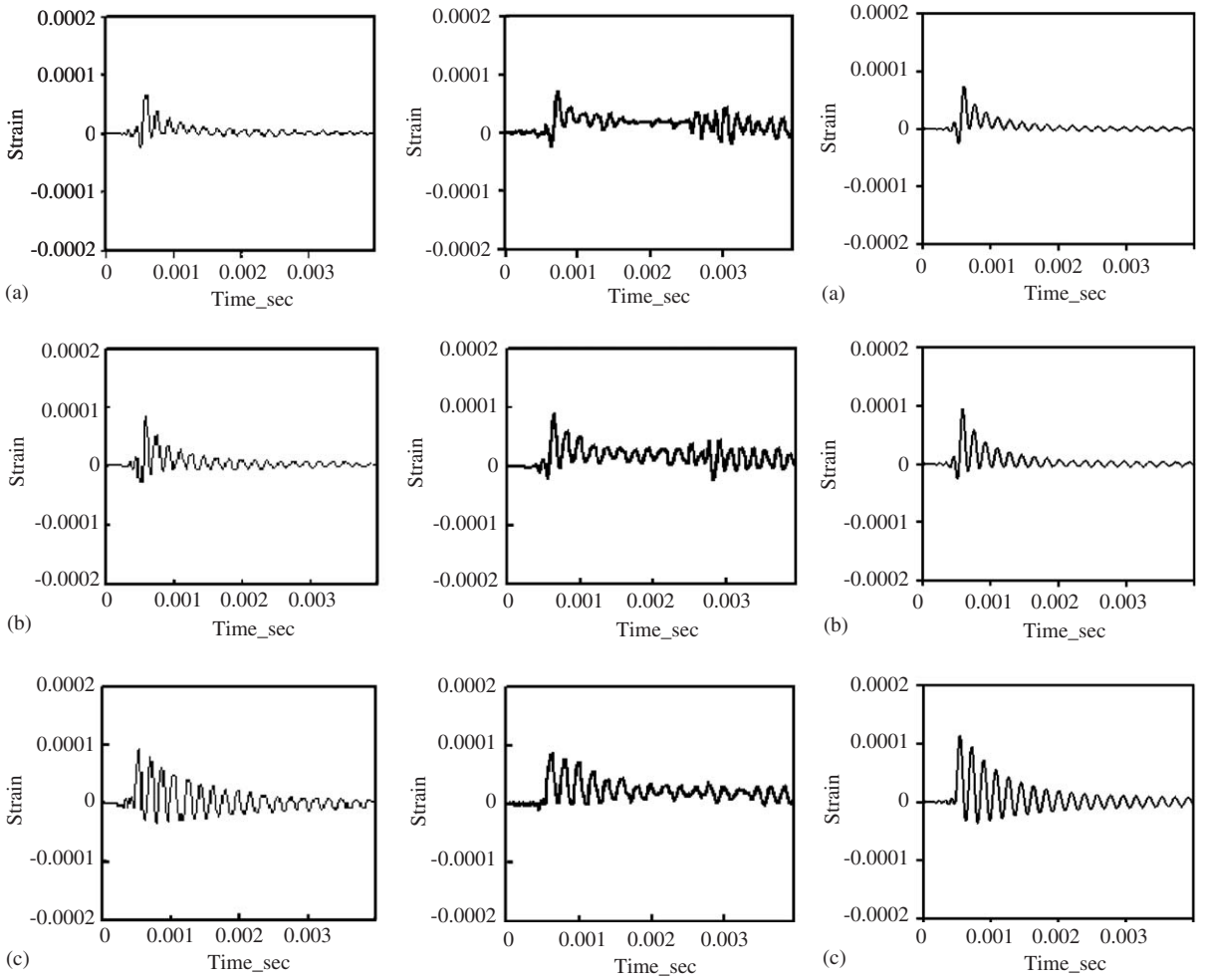

Fig. 11. Left column shows FEM results, right column shows transient model II, and middle column shows experimental strain predictions [1], for gauge 5: (a) detonation velocity of 1400.1 m/s; (b) detonation velocity of 1478.8 m/s and (c) detonation velocity of 1699.7 m/s.

does not exist in this gauge. This strain gauge is located close to the flange at the beginning of the second tube section. The amplification factor is close to 1.56 as a one degree vibrational freedom system. As the distance from the flange at the beginning of the second tube section 2 increases, the flexural waves develop and critical velocity appears in amplification factor.

The amplification factors predicted by the Tang model are obviously not realistic close to the critical speed since a linear model with no damping will always predict an infinite response at the resonant frequency [1]. However, sufficiently far from the resonance, the Tang model correctly predicts that the amplification factor approaches approximately 1 for very subcritical waves and is bounded by 2 for supercritical waves. A maximum amplification factor of 2 is often used for shock or detonation loading. The present results show that near the critical speed, amplification factors larger than 3 are possible in some cases. The growth of the amplification factor with the distance from the flange is clearly shown in both the experimental data and predictions by the transient models. Note that the analytical Tang model gives the same amplification curve for each strain gauge since it assumes a "steady state" situation for a tube of infinite length. The amplifications from the transient model I are relatively high and the peaks do not match with the correct velocities. In general, the amplification factors and critical velocities predicted by transient model II are in better agreement

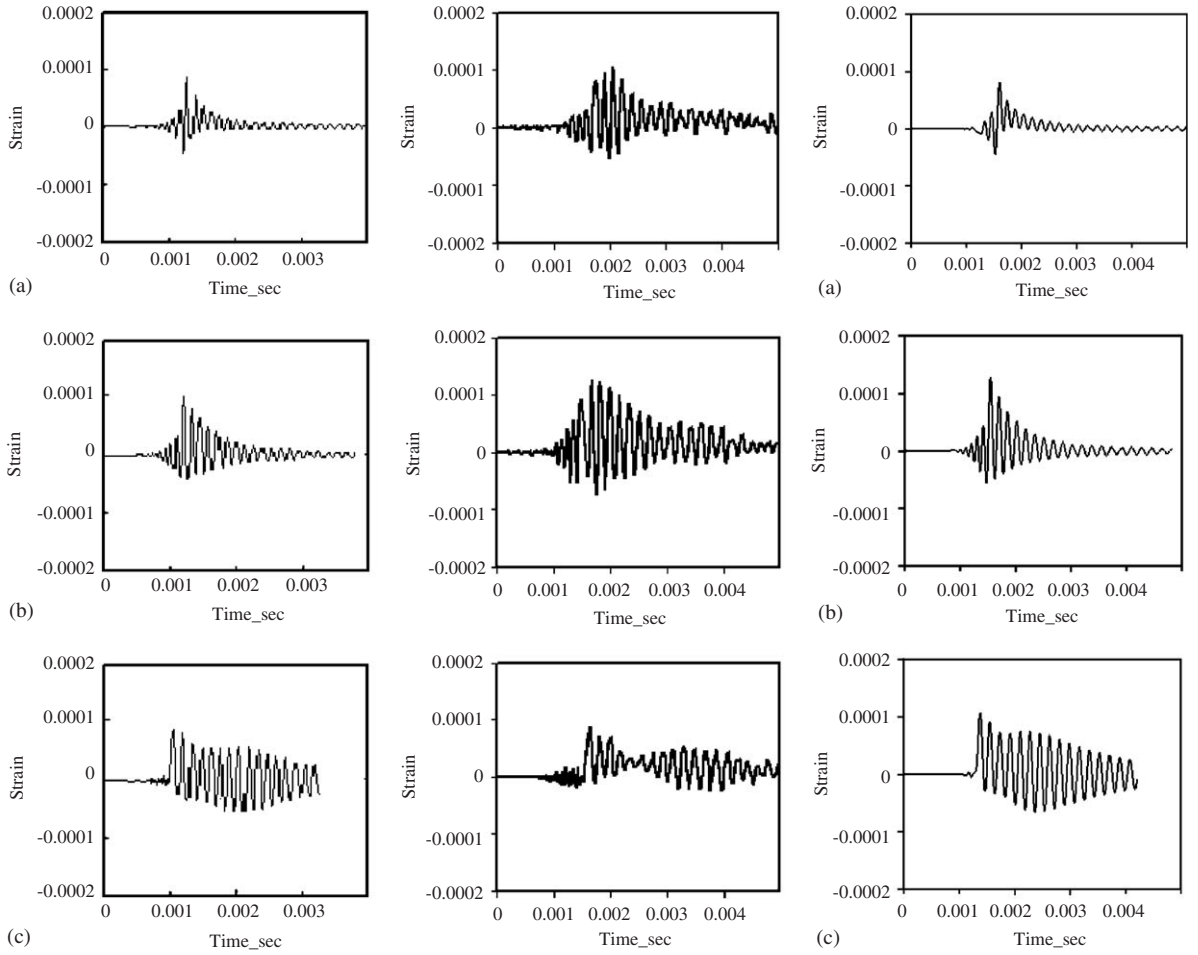

Fig. 12. Left column shows FEM results, right column shows transient model II, and middle column shows experimental strain predictions [1] for gauge 10: (a) detonation velocity of 1400.1 m/s; (b) detonation velocity of 1478.8 m/s and (c) detonation velocity of 1699.7 m/s.

with the experimental results. Of course the best agreement with the experimental results is provided by the FEM simulations. It is clearly seen that amplification factor is a function of velocity and has its *maximum* at critical velocity. In order to precisely calculate the critical velocity, we should look for the conditions that maximize the deflections. These conditions can be found by setting the common denominator of the first and second terms in Eq. (31) equal to zero.

$$\omega_n^2 - \left(\frac{n\pi V}{l}\right)^2 = 0 \Rightarrow V = \frac{\omega_n L}{n\pi}. \tag{35}$$

Now it remains to find the minimum velocity from Eq. (35), which occurs at a particular n. Fig. 14 shows the variation of velocity with mode number according to Eq. (35), which contains a minimum at the mode number 25. Thus, the critical velocity can be calculated from Eq. (35) by setting $n = 25$. The experimental results indicate that the critical velocity of the tube is about 1450 m/s [1]. This is close to the value that was predicted by the analytical Tang model: 1455 m/s. The critical speed predicted by transient model I is higher (1543 m/s) due to the fact that in this model the effects of rotary inertia and transverse shear are neglected. However, transient model II predicts the critical velocity as 1447.5 m/s due to its enhanced formulation. The critical velocity obtained from the finite element simulation is about 1460 m/s.

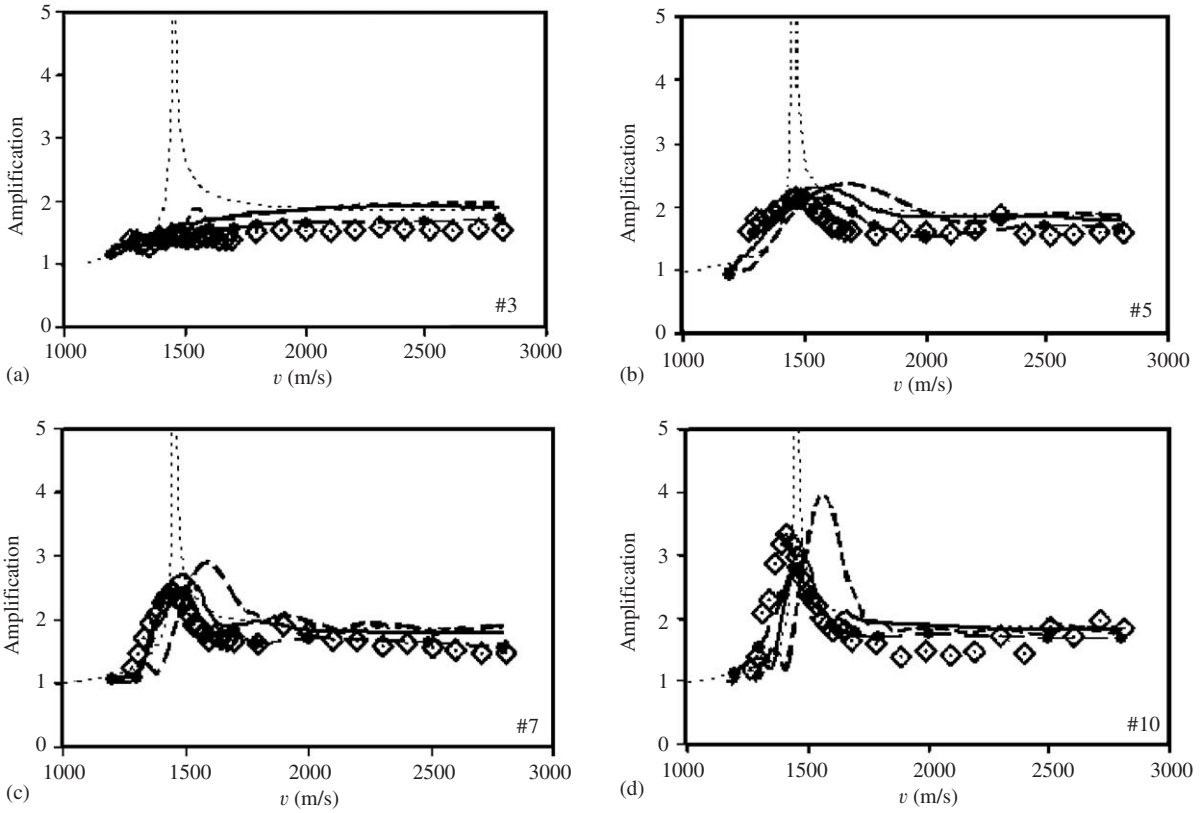

Fig. 13. Amplification factor for the entire range of detonation velocities predicted by FEM, –●–●–; Tang model, - - - -; transient model I, – – – –; transient model II, ——; and the experimental results [1] ◇ for: (a) gauge #3, (b) gauge #5, (c) gauge #7, and (d) gauge #10.

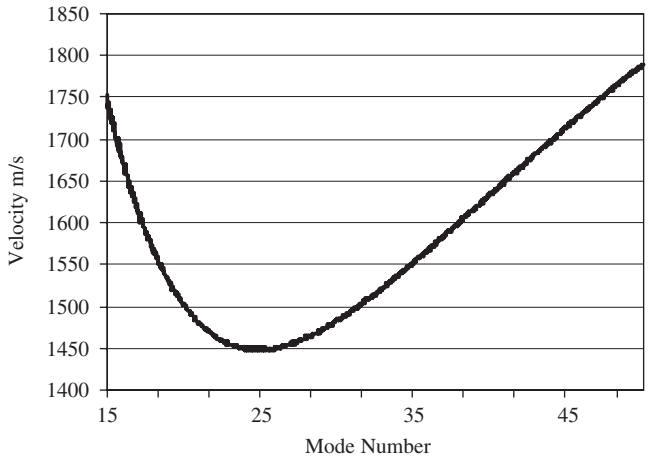

Fig. 14. Variation of velocity with mode number.

5. Conclusions

The following conclusions are drawn from the present investigation:

1. The critical velocity for the detonation tube with the material and geometrical properties shown in Table 1 is predicted by Tang model as 1455 m/s, by transient model I as 1543 m/s, by transient model II as 1447.5 m/s and by FEM as 1460 m/s. The experimental critical velocity is 1450 m/s.

2. The asymptotic values for the amplification factor predicted by the above three models equal 1 for subcritical waves and 2 for supercritical waves.
3. The finite element simulations indicate that if the effects of reflected flexural waves are neglected, the support condition of the tube is not an important factor.
4. Analytical models usually predict amplification factors greater than experimental results. The amplification factors predicted by Tang model are obviously not realistic close to the critical speed. The amplification factors predicted by transient model II are in better agreement with the experimental results, compared to the results obtained from transient model I. In general, the simulations obtained from Model II are in better agreement with the experimental and FEM results. This can be attributed to the consideration of the effects of transverse shear and rotary inertia in the formulation of this model.
5. For design purposes, these analytical models are very useful and can provide initial good estimations which may be further refined with detailed finite element analyses.

References

[1] W.M. Beltman, J.E. Shepherd, Linear elastic response of tubes to internal detonation loading, *Journal of Sound and Vibration* 252 (2002) 617–655.
[2] M.C. De Malherbe, R.D. Wing, A.J. Laderman, A.K. Oppenheim, response of a cylindrical shell to internal blast loading, *Journal of Mechanical Engineering Science* 8 (1966) 91–98.
[3] J.E. Shepherd, Pressure loads and structural response on the BNL high-temperature detonation tube, Technical Report A-3991, Brookhaven National Laboratory, Upton, New York, September 1992.
[4] A. Van de Ven, H. Olivier, H. Grönig, Dynamic structural response of a dust detonation tube, *Seventh International Colloquium on Dust Explosions*, Bergen, 1996.
[5] A. Sperber, H.P. Schildber, S. Schlehlein, Dynamic load on a pipe caused by acetylene detonations—experiments and theoretical approaches, *Journal of Shock and Vibration* 6 (1999) 29–43.
[6] T.E. Simkins, Resonance of flexural waves in gun tubes, Technical Report ARCCB-TR-87008, US Army Armament Research, Development and Engineering Center, Watervliet, NY, July 1987.
[7] T.E. Simkins, G.A. Pflegl, E.G. Stilson, Dynamic strains in a 60 mm gun tube—an experimental study, *Journal of Sound and Vibration* 168 (1993) 549–557.
[8] T.E. Simkins, Amplification of flexural waves in gun tubes, *Journal of Sound and Vibration* 172 (1994) 145–154.
[9] T.E. Simkins, The influence of transient flexural waves on dynamic strains in cylinders, *Journal of Applied Mechanics—Transactions of the American Society of Mechanical Engineers* 62 (1995) 262–265.
[10] W.M. Beltman, E.N. Burcsu, J.E. Shepherd, L. Zuhal, The structural response of tubes to internal shock loading, *Journal of Pressure Vessel Technology* 121 (1999) 315–322.
[11] S. Tang, Dynamic response of a tube under moving pressure, *Proceedings of the American Society of Civil Engineers*, Engineering Mechanics Division, Vol. 5, October 1965, pp. 97–122.
[12] H. Reismann, Response of a pre-stressed cylindrical shell to moving pressure load, in: S. Ostrach, R.H. Scanlon (Eds.), *Eighth Midwest Mechanics Conference*, Pergamon Press, Oxford, 1965, pp. 349–363.
[13] W.M. Beltman, J.E. Shepherd, The structural response of tubes to detonation and shock loading—parts I and II, Technical Report FM98-3, California Institute of Technology, Pasadena, CA, April 1998.
[14] M. Mirzaei, K. Mazaheri, H. Biglari, Analytical modeling of the elastic response of tubes to internal detonation loading, *International Journal of Pressure Vessels and Piping* 82 (2005) 883–895.